Methods, supplementary figures and tables

Performance of ferrite nanoparticles in inductive heating swing adsorption (IHSA): how tailoring material properties can circumvent the design limitations of a system.

Maxim De Belder[a,c,†], Alysson F. Morais[a,d,†], Natan De Vos[a], Luc Van Meervelt[b], Joeri F.M. Denayer[c], Johan A. Martens[a,d] and Eric Breynaert[a,d,*]

[a]Center for Surface Chemistry and Catalysis - Characterization and Application Team (COK-KAT), KU Leuven, 3001 Leuven, Belgium.
[b]Department of Chemistry, KU Leuven, 3001 Leuven, Belgium.
[c]Department of Chemical Engineering, Vrije Universiteit Brussel, 1050 Brussels, Belgium.
[d]NMRCoRe – NMR - X-Ray platform for Convergence Research, KU Leuven, 3001 Leuven, Belgium.
† These authors contributed equally to this work
* Corresponding author: eric.breynaert@kuleuven.be

Contents

SI-1 Clarification on inductive heating mechanisms

Joule heating results from the generation of 'Eddy currents' in macroscopic conductors. Typically, this mechanism prevails in the heating of metallic species. This has been implemented on a large scale, in kitchen appliances around the globe, and in a multitude of industrial applications. In the context of gas separation, however, long-term stability is a legitimate concern. Hence, these species are disregarded due to their inadequate oxidative and chemical stability.

The other three mechanisms of inductive heating occur in ferro- and ferrimagnetic species. When magnetic nanoparticles are dispersed as a ferrofluid, they are capable of dissipating heat via Brownian- and Néel relaxation. The former involves the physical rotation of the particles in the fluid, generating heat via friction. The latter implies a reorientation of the magnetization inside the particle against the energy barrier associated with the easy axis of magnetization. However, these mechanisms will not be present in the heating of a solid phase, such as a sorbent. The third mechanism, present in solid-state ferro- and ferri-magnetic particles, is hysteresis loss. In this last mechanism, heat is generated via the realignment of magnetic domains along the direction of the externally applied field.

SI-2 Materials and Methods

Adapted procedure from Maaz et al. and Surendra et al..[1,2] All chemicals and reagents were of analytical grade and used without further purification. The precursor solutions were made of 1 mol L^{-1} of the metal nitrates in the stoichiometric ratio corresponding with the final composition of the ferrite. For cobalt ferrite ($CoFe_2O_4$), the precursor consisted of Iron (III) nitrate nonahydrate ($Fe(NO_3)_3 \cdot 9\ H_2O$, Fisher) and Cobalt (II) nitrate hexahydrate ($Co(NO_3)_2 \cdot 6\ H_2O$, AlfaAesar). For nickel ferrite ($NiFe_2O_4$), the precursor consisted of Iron (III) nitrate nonahydrate and Nickel (II) nitrate hexahydrate ($Ni(NO_3)_2 \cdot 6\ H_2O$, Fisher). For cobalt-substituted nickel ferrites

($Ni_xCo_{1-x}Fe_2O_4$), the precursor solution consisted also of Iron (III) nitrate nonahydrate ($Fe(NO_3)_3 \cdot 9\ H_2O$, Fisher), and a mixture of Cobalt (II) nitrate hexahydrate ($Co(NO_3)_2 \cdot 6\ H_2O$, AlfaAesar) and Nickel (II) nitrate hexahydrate ($Ni(NO_3)_2 \cdot 6\ H_2O$, Fisher).

Co-precipitation was carried out by dropwise addition of the precursor solution to 200 mL of Milli-Q H_2O. 100 µL of oleic acid (Acros) was added to mitigate aggregation in the precipitation stage. The addition is done via a perfusion pump and a 25 mL syringe at a rate of 10 mL/h. The pH is kept constant throughout the precipitation stage via the addition of 1 M NaOH.

Upon completion, the precipitate is consecutively aged at 80°C for 1h in dynamic conditions. After cooling to room temperature, the precipitate is washed twice with Milli-Q H_2O and once with absolute ethanol. The wet precipitate was dried at 60°C for 24h in the oven. Finally, the precipitate is ground and subsequently calcined at a temperature of 600 °C during 6h.

All samples were structurally analysed using powder X-ray diffraction with Mo Kα radiation (Agilent Supernova diffractometer). The size and morphology of the particles were characterized on a transmission electron microscope (ARM200F by JEOL) operating at 200 kV. Elemental composition is evaluated using ICP-OES (Varian 720-ES) with cooled cone interface and oxygen-free optics. The corresponding lines for Co, Fe, and Ni were 228.615, 238.204, and 231.604 respectively. The magnetic characterization of the resulting particles was performed on a VSM-SQUID (MPMS-3 by Quantum Design) by measuring the hysteresis loops at 300 K and with a maximum field of ±70 kOe.

Table S1: Nomenclature and bulk composition of the produced samples, as derived from ICP-OES data.

	Nominal			Experimental			
Name	**100*Ni/(Ni+Co)**	**100*Co/(Ni+Co)**	**Formula**	**Co wt%**	**Fe wt%**	**Ni wt%**	**Formula**
CF	0	100	$CoFe_2O_4$	4.687	3.689	0.015	$CoFe_2O_4$
NCF 80	80	20	$Ni_{0.80}Co_{0.20}Fe_2O_4$	2.821	14.919	11.056	$Ni_{0.80}Co_{0.20}Fe_2O_4$
NCF 90	90	10	$Ni_{0.90}Co_{0.10}Fe_2O_4$	1.025	13.082	8.884	$Ni_{0.90}Co_{0.10}Fe_2O_4$
NCF 95	95	5	$Ni_{0.95}Co_{0.05}Fe_2O_4$	0.397	8.901	7.191	$Ni_{0.95}Co_{0.05}Fe_2O_4$
NF	100	0	$NiFe_2O_4$	0.006	5.069	4.034	$NiFe_2O_4$

To determine the inductive heating performance, the particles were submerged in 8.68 mL of milli-Q H_2O in a 10 mL glass vial. Testing was conducted on an Ambrell 8310 with a coil with a length of 7 cm, 8 turns, and an outer diameter of 3.8 cm. The field was operated at a frequency of 248 kHz and at different amplitudes (99, 136, 158, 200, 226, and 257 Oe). The specific absorption rate (SAR) in W/g was calculated based on the initial temperature change using equations SI-1-3, with $(mC_p)_{tot}$ of 50 J/K:

$$\left.\frac{dT}{dt}\right|_{t=0} = \frac{Q}{(mC_P)_{tot}} \tag{SI-1}$$

$$(mC_P)_{tot} = (mC_P)_{water} + (mC_P)_{vial} + (mC_P)_{FNP} \tag{SI-2}$$

$$SAR = \frac{Q}{m_{FNP}} \tag{SI-3}$$

SI-3 Modelling

Integrating the area between the hysteresis described by Eq. 3 in the main text, the amount of heat that can be generated through hysteresis losses is:

$$\frac{SAR.\rho}{\mu_0 V M_S f} = \frac{2}{\alpha} ln\left[\frac{\cosh \alpha(h_{max} + H_C)}{\cosh \alpha(h_{max} - H_C)}\right] - 2h_{max}\{tanh[\alpha(h_{max} + H_C)] - tanh[\alpha(h_{max} - H_C)]\} \tag{SI-4}$$

where ρ is the density of the material and f is the frequency of the oscillating magnetic field.

To analyse equation SI-4 for a system where h_{max} is fixed, we define the variables:

$$A = \alpha h_{max}$$

$$\eta = {}^{H_C}/_{h_{max}}$$

And Eq SI-4 can be rewritten as:

$$\frac{SAR.\rho}{4\,\mu_0 M_S h_{max}\,f} = \frac{1}{2A} ln\left[\frac{\cosh A(1+\eta)}{\cosh A(1-\eta)}\right] - \frac{1}{2}\{\tanh[A(1+\eta] - \tan[A(1-\eta]\} \quad \text{(SI-5)}$$

To analyse equation SI-4 for a system where H_C *and* α are fixed, we define the variables:

$$\beta = \alpha H_C$$

$$\gamma = {}^{h_{max}}/_{H_C}$$

And Eq SI-4 can be rewritten as:

$$\frac{SAR.\rho}{4\,\mu_0 M_S H_C\,f} = \frac{1}{2\beta} ln\left[\frac{\cos\beta(\gamma+1)}{\cos\beta(\gamma-1)}\right] - \frac{\gamma}{2}\{\tan\beta(\gamma+1) - \tan\beta(\gamma-1)\} \quad \text{(SI-6)}$$

SI-4 X-ray diffraction

The PXRD patterns of the ferrite samples shown on **Figure S1** confirm the formation of the spinel ferrite phases, as evidenced by the presence of the characteristic peaks. Le Bail fitting confirmed the characteristic cubic unit cell of a spinel ferrite, with lattice parameters a = b = c = 8.318 Å

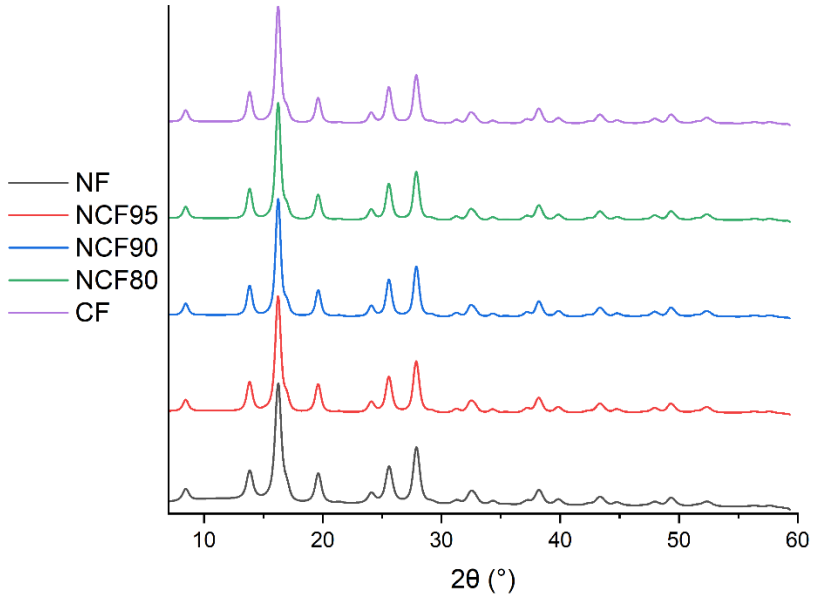

Figure S1: X-ray diffractograms of the samples (measured with Mo Kα radiation)

SI-5 Additional magnetization information

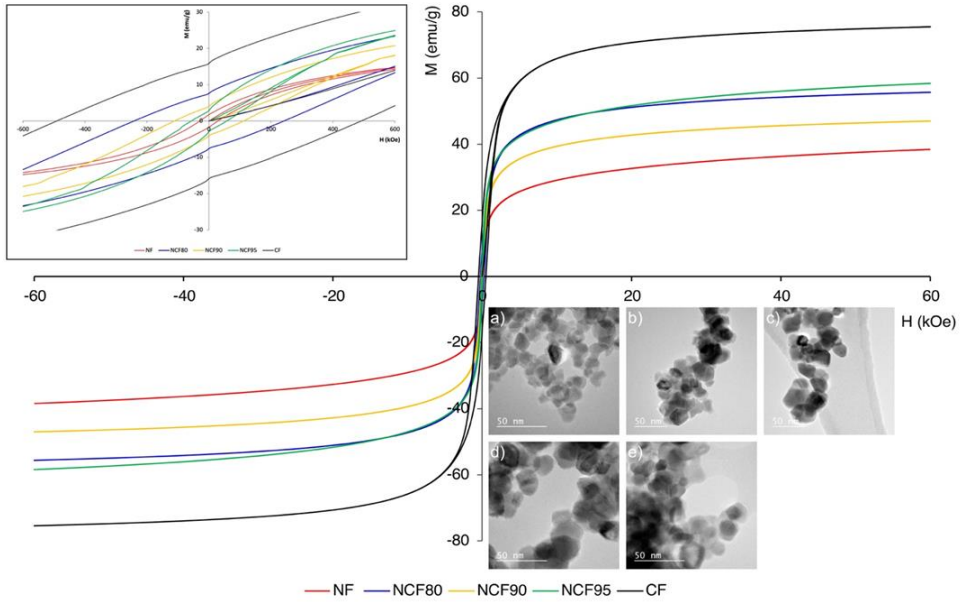

Figure S2: Full magnetization curve of the samples, Zoomed-in section of magnetization curve at low field strengths, and TEM images of samples. a) CF, b) NCF80, c) NCF90, d) NCF95, and e) NF

SI-6 SAR values

Table S2: SAR values for different ferrite nanoparticles measured at varying field strengths alternated at 248 kHz.

						SAR (W/g)					
						field strengths (in Oe)					
Name	**%Ni**	**%Co**	**M_S (emu/g)**	**H_C (Oe)**	**α (1/kOe)**	99.0	135.7	158.3	200.7	226.2	257.3
CF	0	100	75.47	490.69	0.5	0.5	1.6	1.7	3.6	5.8	8.2
NCF 80	80	20	55.63	241.37	0.65	0.3	0.9	1.0	2.4	4.0	5.5
NCF 90	90	10	47.00	111.12	0.86	0.4	1.1	1.5	4.8	8.3	12.3
NCF 95	95	5	58.43	56.67	0.99	0.7	2.2	3.5	8.4	13.6	21.4
NF	100	0	38.44	29.18	1.26	4.6	10.6	15.6	25.9	30.2	43.8

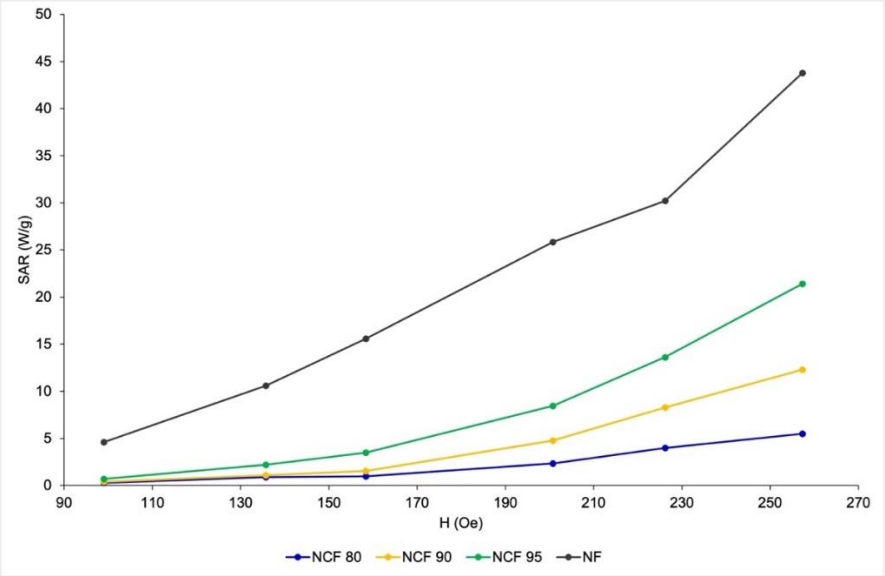

Figure S3: SAR as a function of external field strength.

Table S3: A comparison of different works in literature employing ferrite susceptors for inductive heating.

Author	Susceptor	Material	M_S (emu/g)	H_C (Oe)	Particle size (nm)	h_{max} (Oe)	f (kHz)	SAR (W/g)	SAR.f^{-1} ζ (mJ/g)
Present work	$NiFe_2O_4$	Ni-ferrite	38.4	29.2	25	257	248	43.8	177
Bellusci[1]	Fe_3O_4	MOF + 17% magnetite	84.00	40	33.2	126	190	9.4	49.5
Newport[2]	Fe_2O_3	13X + 20% hematite	NA	NA	5000	324	– #	53.2	– #
Sadiq[3,*]	$MgFe_2O_4$	Mg-ferrite*	67	105	13.6	210	– #	32.4	– #
						320		46.7	– #
Ghasemi[4]	$Cu_{0.2}Cd_{0.8}Fe_2O_4$	Cu/Cd-ferrite	20	10	13.8	384	340	0.7	2.06

* In their work, Sadiq et al. employ a composite consisting of UiO-66 and $MgFe_2O_4$ for the eventual IHSA application. In contrast to the other works, detailed information about the unincorporated susceptor particle is provided. ζ Calculated by us to allow comparison between different references. Calculated using the information provided in the respective references. According to Eq. 1-2 from the main text, this quantity corresponds to the heat generated during one field cycling. # Frequency not specified by the authors.

SI-7 Density

The density of each of the materials was estimated via the nominal chemical formula and the unit cell volume derived from their crystal structure. The results are listed in **Table S5**.

Table S4: Densities of the different ferrite species

Sample	NF	NCF80	NCF90	NCF95	CF
Formula	$NiFe_2O_4$	$Ni_{0.80}Co_{0.20}Fe_2O_4$	$Ni_{0.90}Co_{0.10}Fe_2O_4$	$Ni_{0.95}Co_{0.05}Fe_2O_4$	$CoFe_2O_4$
Density# (g/cm^3)	5.1854	5.1864	5.1859	5.1857	5.1907

Density evaluated via the unit cell volume and the mass of its contents.

SI-8 Thermogravimetric data

The formation of a thermally stable nickel ferrite out of a hydroxide is precursor is attested by a thermogravimetric analysis.

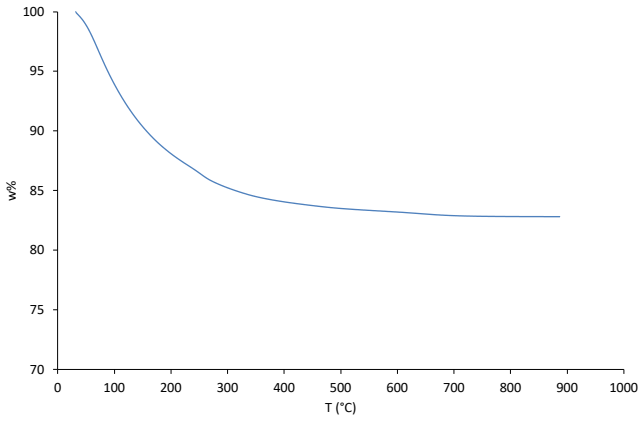

Figure S4: The thermogravimetric curve of a Ni/Fe hydroxide used as a precursor for the fabrication of $NiFe_2O_4$ ferrites.

References

1 K. Maaz, S. Karim, A. Mumtaz, S. K. Hasanain, J. Liu and J. L. Duan, *J Magn Magn Mater*, 2009, **321**, 1838–1842.
2 M. K. Surendra, R. Dutta and M. S. Ramachandra Rao, *Mater Res Express*, , DOI:10.1088/2053-1591/1/2/026107.
3 M. Bellusci, M. Albino, A. Masi, D. Peddis, C. Innocenti and F. Varsano, *Mater Chem Phys*, 2024, **311**, 128525.
4 K. Newport, K. Baamran, A. A. Rownaghi and F. Rezaei, *Ind Eng Chem Res*, 2022, **61**, 18843–18853.
5 M. M. Sadiq, H. Li, A. J. Hill, P. Falcaro, M. R. Hill and K. Suzuki, *Chemistry of Materials*, 2016, **28**, 6219–6226.
6 R. Ghasemi, J. Echeverría, J. I. Pérez-Landazábal, J. J. Beato-Lopez, M. Naseri and C. Gómez-Polo, *J Magn Magn Mater*, 2020, **499**, 166201.